Geology and Chemistry of the El Abuelo Calcic Fe-skarn and Related Cu-(Ag)-Bearing Hydrothermal Veins, Chubut Province, Southern Argentina

M.E. LANFRANCHINI[1,†], R.E. DE BARRIO[2], AND R.O. ETCHEVERRY[1]

Abstract — The El Abuelo Ca-Fe-magnetite skarn and related hydrothermal quartz veins are located at Cerro Pepita Hill, in southwestern Chubut province of southern Argentina, 1700 km southwest of Buenos Aires. These deposits are developed in a continental magmatic arc environment linked to the Andean orogeny. Iron skarn mineralization is mainly hosted by an Upper Jurassic to Early Cretaceous sedimentary sequence interbedded with Upper Jurassic basaltic andesite, and is spatially associated with Early Cretaceous calc-alkaline dikes. Ore grades vary between 40 and 63 wt.% Fe. In addition, anomalous metal contents (>10 000 ppm Cu and up to 81 g/t Ag) are present in the hydrothermal quartz veins.

At least three paragenetic mineral assemblages have been identified in the El Abuelo exoskarn: (1) amphibole > epidote ± chlorite ± quartz, formed by isochemical contact metamorphism; (2) Fe-clinopyroxene ± Ca-garnet, formed during prograde metasomatic anhydrous exoskarn formation; and (3) actinolite ± epidote ± chlorite ± quartz ± magnetite > titanite, resulting from hydrous retrograde alteration of exoskarn. Endoskarn alteration involved an early Mg-Fe-clinopyroxene ± Fe-garnet assemblage followed by retrograde actinolite replacement of pyroxene. Lower temperature hydrothermal alteration related to quartz veins was superimposed on the skarn assemblages, showing an innermost sericite ± adularia ± pyrite ± chalcopyrite assemblage and an external propylitic halo.

Some metallogenic characteristics of the mineralization and the geological setting resemble those in several iron oxide copper-gold deposits elsewhere in the world. **© 2007 Canadian Institute of Mining, Metallurgy and Petroleum. All rights reserved.**

Key Words: Calcic Fe-skarn, hydrothermal veins, Lower Cretaceous, Argentina.

Sommaire — Le skarn à Ca-Fe-magnétite et les veines de quartz hydrothermal associées sont situés à Cerro Pepita Hill, dans le sud-ouest de la province de Chubut au sud de l'Argentine, à 1700 km de Buenos Aires. Ces gîtes se développent dans un contexte d'arc magmatique continental associé à l'orogenèse Andine. Les minéralisations de type skarn ferrifère se retrouvent principalement dans une séquence sédimentaire d'âge Jurassique Supérieur à Crétacé précoce interlitée avec de l'andésite basaltique du Jurassique Supérieur, et elle présente une association spatiale avec des dykes calco-alcalins du Crétacé précoce. La teneur du minerai varie de 40 à 63 % poids Fe. De plus, des teneurs anomales en métaux (>10 000 ppm Cu et atteignant 81 g/t Ag) sont notées dans les veines de quartz hydrothermal.

Au moins trois assemblages minéraux ont été identifiés dans l'exoskarn d'El Abuelo : (1) amphibole > épidote ± chlorite ± quartz, issus d'un métamorphisme de contact isochimique; (2) Clinopyroxène-Fe ± grenat-Ca, contemporains de la formation de l'exoskarn métasomatique prograde anhydre; et (3) actinolite ± épidote ± chlorite ± quartz ± magnétite > titanite, résultant de l'altération rétrograde hydratée de l'exoskarn. La formation de l'altération de l'endoskarn a impliqué un assemblage précoce constitué de Clinopyroxene-Mg-Fe ± grenat-Fe suivi du remplacement rétrograde du pyroxène par l'actinolite. L'altération hydrothermale de basse température associée aux veines de quartz se superpose aux assemblages du skarn, montrant une zone interne marquée par l'assemblage séricite ± adulaire ± pyrite ± chalcopyrite et un halo propylitique externe.

Certaines caractéristiques métallogéniques de ces minéralisations et de leur contexte géologique ressemblent à celles de plusieurs gîtes d'oxyde de fer-cuivre-or ailleurs dans le monde. **© 2007 Canadian Institute of Mining, Metallurgy and Petroleum. All rights reserved.**

---

[1] Consejo Nacional de Investigaciones Científicas y Técnicas (CONICET), Instituto de Recursos Minerales (INREMI), FCN y M, UNLP, Calle 64 N° 3 entre 119 y 120, (1900) La Plata, Argentina.

[2] Instituto de Recursos Minerales (INREMI), FCN y M, UNLP, Calle 64 N° 3 entre 119 y 120, (1900) La Plata, Argentina.

[†] *Corresponding Author:* E-mail: mlanfranchini@inremi.unlp.edu.ar

Introduction

Many of the numerous skarn deposits in Argentina define a 1600 km long belt (24º–38°S) along the western margin of the Andean Cordillera and related geological provinces (Franchini, 2005). Most of the known skarn districts occur along the Cordillera Principal of southwestern Mendoza and northwestern Neuquén provinces (34°–38°S). The deposits are associated with Tertiary intrusions, which display typical subduction-related geochemical features (calc-alkaline signature with intermediate to acid composition), emplaced at shallow levels (Méndez et al., 1995; Franchini and Dawson, 1999; Franchini et al., 2000, 2005).

The only mineralized skarn currently known in the Argentinean Andean cordillera south of 38°S is the El Abuelo deposit, located in southwestern Chubut province (44º55′30″S, 70º55′00″W). Unlike all the other Tertiary-age skarns further north, the El Abuelo deposit is associated with Lower Cretaceous rhyolite and dacite porphyry dikes.

This paper summarizes the geochemistry of the related Mesozoic igneous rocks, as well as the geology, alteration, and mineralization of the El Abuelo skarn and its associ-ated hydrothermal veins (Fig. 1). The relationship between the evolving hydrothermal fluids and the resulting altera-tion mineral assemblages is underlined and a petrogenetic scheme is proposed. The comparable metallogenic charac-teristics between the El Abuelo Fe skarn and other skarn deposits of Argentina and Chile are also noted, as well as some relevant features of iron oxide copper-gold (IOCG) deposits described in the literature.

Previous Work

No geochemical exploration data are available for the El Abuelo deposit, despite iron mining activities in the dis-trict carried out between 1940 and 1960. The deposit was first discovered by Hayase et al. (1972), and Medina and Maisterrena (1981) later suggested a close relationship be-tween the hydrothermal mineralization and rhyolitic rocks, generated during the Jurassic–Cretaceous volcanic activ-ity. Dawson et al. (2000) observed massive magnetite with garnet in the El Abuelo mine, and the chemistry of Mn-hedenbergite was described by Hayase and Labudía (1972) and Canafoglia et al. (2002). More recently, Lanfranchini (2004) characterized some geological and mineralogical
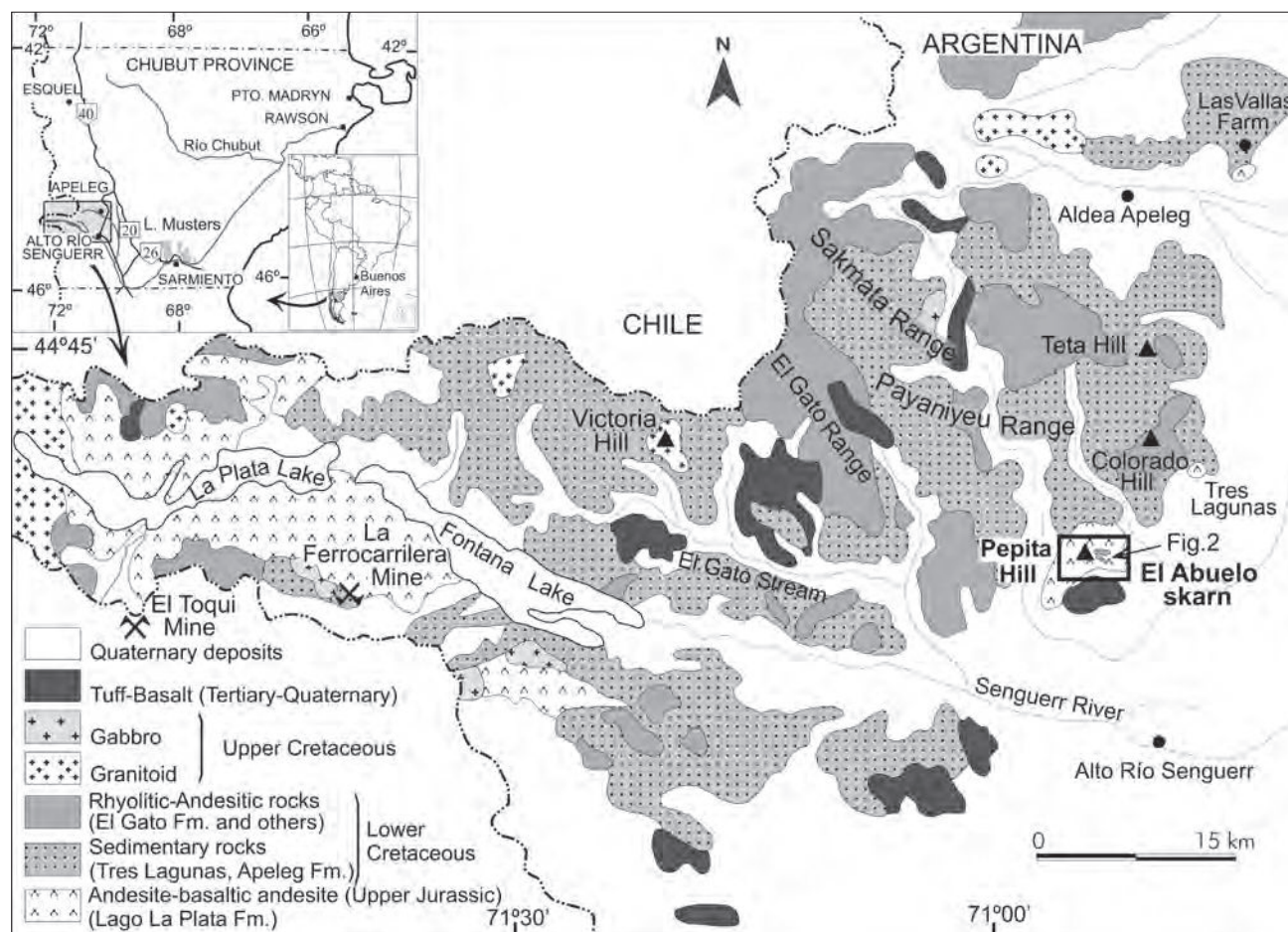

Fig. 1. Regional geologic map and geographic location of the study area (simplified from Ramos, 1981; Ploszkiewicz, 1987).

aspects of the skarn.

Analytical Methods

Major and trace element compositions of whole-rock samples were obtained by inductively coupled plasma–emission spectrometry (ICP-ES), inductively coupled plasma–mass spectrometry (ICP-MS), and instrumental neutron activation analysis (INAA) at Alex Stewart Assayers Argentina S.A., OMAC Laboratories (Ireland), and Actlabs Ltd. (Canada), respectively.

Electron microprobe analyses were obtained using a Cameca Camebax SX-50 at the Departamento de Geología, Universidad de Oviedo, Spain. Operating conditions were a 15 to 20 kV accelerating voltage, beam current of 15 to 20 mA, and beam size of 1 to 2 μm. Natural standards were certified by MAC (Micro Analysis Consultants Ltd., United Kingdom).

Representative samples of silicates and sulfides were selected for stable isotope determinations and were performed at the Laboratorio de Isótopos Estables, Facultad de Ciencias, Universidad de Salamanca, Spain. Extracted gases were analyzed in a VG Isotech Micromass SIRA-II spectrometer, equipped with a cryogenic dispositive (cold finger). The isotopic ratios measured were reported in the conventional δ notation (‰).

Oxygen and hydrogen gas extractions were performed by conventional methods (Clayton and Mayeda, 1963). The isotope ratios are given relative to the Standard Mean Ocean Water (SMOW) standard, with an analytical error of ±0.8‰ for $\delta^{18}O$, and ±1‰ for δD.

SO_2 gas extraction was performed by conventional methods (Robinson and Kusakabe, 1975). Sulfur compositions are reported in delta notation relative to the CDT standard ($\delta^{34}S$), with an analytical error of ±0.27‰.

Geological Setting

During the Mesozoic Andean orogeny in southern Argentina, widespread calc-alkaline magmatism was developed in a Jurassic–Cretaceous volcanic arc (Fig. 1). This continental arc formed as a result of the convergent eastward subduction of the Nazca Plate beneath the South American Plate (Sillitoe, 1974; Ramos, 1993).

The Lago La Plata Formation is the oldest unit in the study area. It comprises dark porphyritic volcanic rocks of Middle to Upper Jurassic age (Ra-

mos, 1976). The upper part of the basaltic andesite flows is interlayered with the lower section of the Tres Lagunas Formation, a marine sedimentary sequence of Late Jurassic–Early Cretaceous age (Ploszkiewicz and Ramos, 1977). Subsequently, an extensive, thick, quartz sandstone deltaic system, the Apeleg Formation, was deposited in southwestern Chubut province (Ploszkiewicz and Ramos, 1977).

During the Early Cretaceous, the volcano-sedimentary succession was intruded by a 900 m-wide porphyritic rhyolitic to dacitic body, which correlates with the El Gato Formation (Ploszkiewicz and Ramos, 1977). This body passes out into several near-vertical crosscutting porphyritic rhyolitic to dacitic dikes. They exhibit moderate brittle fracturing with a hydrothermal alteration halo, which suggests an intermediate to shallow level of intrusion. K-Ar whole-rock dating on a dacitic dike yielded an age of 125 ± 10 Ma (Ramos, 1981).

The field relationships and geochemistry (Table 1) suggest that the dikes are derived from two different, but con-

Table 1. Representative Major and Trace Element Chemical Analyses of Selected Igneous Units: Pepita Hill

Samples		L. La Plata Andesites			Rhyolite Dikes				Dacitic Dikes		
		45	110	4265	79	12	13	4257	6	8	4256
SiO_2	wt %	54.61	50.50	48.50	75.47	76.30	75.50	75.70	69.90	68.20	70.30
TiO_2		0.83	0.66	1.07	0.04	0.05	0.04	0.04	0.32	0.30	0.30
Al_2O_3		17.76	16.14	16.86	12.26	12.70	12.89	13.24	15.65	15.05	15.24
Fe_2O_3		7.87	9.27	8.97	2.51	0.69	0.69	1.44	3.25	2.79	3.68
MnO		0.14	0.13	0.29	0.06	0.02	0.02	0.06	0.06	0.03	0.07
MgO		4.71	6.85	7.42	0.15	0.14	0.07	0.15	0.72	0.58	0.75
CaO		6.99	9.79	14.68	0.87	1.02	1.44	0.54	2.98	3.45	2.09
Na_2O		2.95	1.38	1.30	3.78	4.20	4.39	2.72	3.43	3.30	4.13
K_2O		1.19	0.22	0.17	3.20	2.95	2.74	5.29	3.29	3.68	3.39
P_2O_5		0.11	0.07	0.28	0.03	<0.01	<0.01	0.04	0.14	0.12	0.52
Cr_2O_3		0.01	0.03	0.04	0.01	0.02	0.02	<0.001	0.02	0.02	<0.001
LOI		3.18	4.32	1.14	1.73	0.77	0.64	0.89	1.86	1.66	1.09
SUM		100.35	99.36	100.72	100.11	98.86	98.44	100.11	101.62	99.18	101.56
Au	ppb	–	–	–	–	<2*	<2*	<2*	<2*	8*	8*
Ag	ppm	–	–	–	–	<5*	<5*	<5*	<5*	<5*	<5*
As		–	–	27	–	<0.5*	1.3*	4.3*	<0.5*	1.9*	2*
Ba		259	167	33	667	608	631	726	664	844	774
Ce		27	33	–	23	33	33	20	50	49	40
Cr		50	116	221	55	68*	85*	111*	94*	84*	122*
La		13	15	10	13	18	18	16	26	26	32
Mo		–	–	4	–	<1*	<1*	<1*	<1*	<1*	<1*
Nb		4	5	2	8	8	9	8	9	9	7
Rb		60	5	–	119	100	83	178*	109	97	101*
Sc		26	35	32	1	14*	14*	14*	3	3	3*
Se		<10	<10	<10	<10	<3*	<3*	<3*	<3*	<3*	<3*
Sn		3	2	<20	3	3	4	<20	1	2	<20
Sr		347	218	352	119	205	214	91	283	315	222
Th		5	6	–	12	11.1*	10.3*	10.4*	10.3*	10.6*	10.9*
U		1	1	–	2	3	3	3.1*	3	3	2
V		208	187	296	8	2	11	4	32	19	20
W		1.1	3.1	<20	<0.5	7*	8*	8*	8*	4*	11*
Y		19	25	21	13	19	19	16	20	20	21
Zr		31	9	56	22	56	54	56	147	139	149
Rb/Sr		0.17	0.02	–	1	0.49	0.39	1.96	0.38	0.31	0.45

Note

Samples analyzed by Alex Stewart (Assayers) Argentina S.A. and OMAC Laboratories (Ireland), except those marked *, which were analyzed by Activation Laboratories, Ontario, Canada.
– = not analyzed.
See Fig. 2 for sample locations.

secutive intrusive events. The felsic ones are the least altered. They contain bipyramidal quartz phenocrysts up to 5 mm in length, as well as Carlsbad twinned K feldspar phenocrysts, plagioclase, trace biotite, and Fe-oxides, with accessory apatite and titanite in a felsic groundmass. The dacitic dike contains intermediate composition plagioclase and strongly altered mafic (amphibole?) phenocrysts enclosed in a pilotaxitic groundmass.

The Early Cretaceous tectonic environment was extensional, and was marked by basement block-faulting with regional ESE/SE-striking subvertical fractures. A change to a compressional regime during the later Miocene resulted in reactivation of these fractures, causing tectonic inversion and crustal shortening (Folguera et al., 2000).

Fig. 2. Detailed geologic map of the Pepita Hill area.

El Abuelo Skarn

Surface exposures of the El Abuelo magnetite skarn deposit occur over a $0.75 \ km^2$ area along Pepita Hill (Figs. 1, 2). It is mainly hosted by calcareous sandstone and shale of the Jurassic–Cretaceous Tres Lagunas Formation, but also occurs in the basaltic andesite of Lago La Plata Formation. Later hydrothermal veins cut the skarn-altered sequence. The El Solcito hydrothermal vein, which occurs some 500 m north of the skarn, is almost 300 m long and is hosted by another sedimentary facies, comprising green siliciclastic sandstone of the Tres Lagunas Formation. Both the El Abuelo and El Solcito mineralizations have been poorly explored, although they have been mined in small surface workings named L1 to L11 on El Abuelo deposit (Fig. 2). Angelelli (1984) notes that ore grades vary between 40 and 63 wt.% Fe in the El Abuelo mine.

Close to the skarn deposit, the basaltic andesite of the Lago La Plata Formation forms small outcrops (Lanfranchini, 2002). These volcanic rocks contain pale green pyroxene and plagioclase ($An_{50–52}$) phenocrysts, enclosed in a groundmass displaying pilotaxitic texture. Chemical analyses of less altered samples (Table 1) show compositions of 48.5 to 54.6 wt.% Si_2O, and 1.5 to 4.1 wt.% K_2O + Na_2O. Discrimination plots (Fig. 3a–c) show that they fall into the basalt and basaltic andesite fields.

The Tres Lagunas Formation formed in small basins characterized by restricted shallow marine environments. Thus, these rocks form isolated small exposures, and the beds, ranging between 0.40 and 0.50 m thick, dip 25°N. The formation comprises calcareous-siliciclastic rocks, interbedded with black shale and brownish to greenish sandstone.

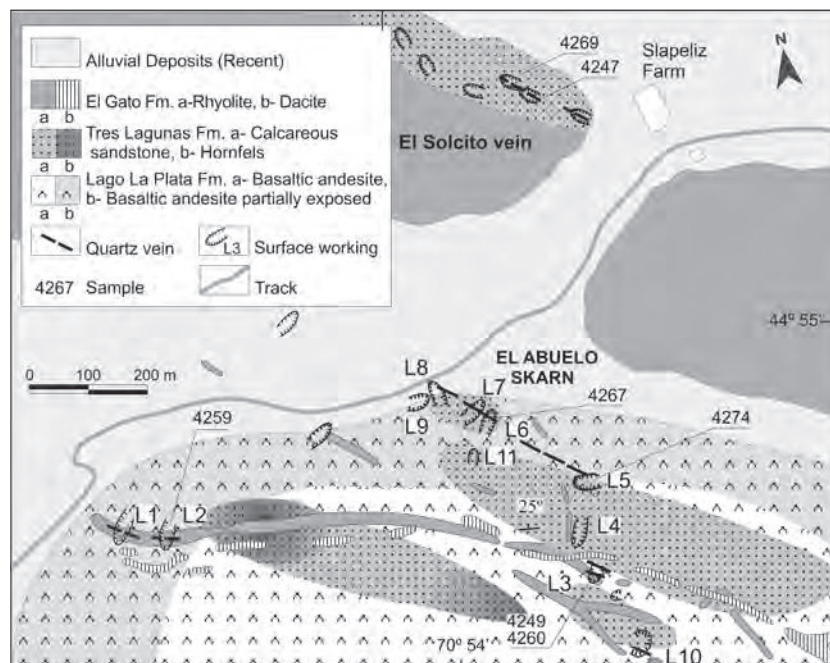The ESE-striking rhyolitic and dacitic dikes in the El Gato Formation, which intrude the volcano-sedimentary sequence, are 0.5 to 5.0 m thick, and up to 900 m long. The older rhyolitic dikes are cut by the dacitic dike. Geochemical plots show the El Gato igneous rocks are of rhyodacite/dacite and rhyolite composition (Fig. 3a–c). Low Nb/Y values (Fig. 3c) are consistent with the subalkaline nature of this igneous suite. In addition, Rb versus Nb+Y tectonic discrimination plots after Pearce et al. (1984) show these rocks fall within the volcanic arc field (Fig. 3d).

Intrusion of the dikes resulted in an irregular and discontinuous thermal hornfels halo. Hornfels occurs at a few small, isolated outcrops, and contacts are not exposed, making it difficult to establish a spatial relationship with the metasomatic halo. This aureole is restricted to the immediate surroundings of the dikes, especially at places near surface workings L2 and L3 (Fig. 2).

Alteration in Igneous and Sedimentary Rocks (Iron Oxide Stage)

Metasomatism of the dacitic dike produced an endoskarn mineral assemblage along the contact with the sedimentary rocks, which is only observed in L3. Massive aggregates of diopsidic-hedenbergitic pyroxene and andraditic garnet endoskarn, a few centimeters thick (Tables 2, 3), almost entirely replace the primary igneous mineralogy. The clinopyroxene is partial to totally retrograded to actinolite.

The rhyolitic dikes are only weakly skarn altered and show a thin halo a few centimeters thick, close to the exoskarn contact (L3). This replacement consists of coarse-grained idiomorphic epidote and quartz.

Contact metamorphism associated with the dacitic dike caused weak isochemical recrystallization of the Tres Lagunas Formation wall rock, resulting a fine-grained,
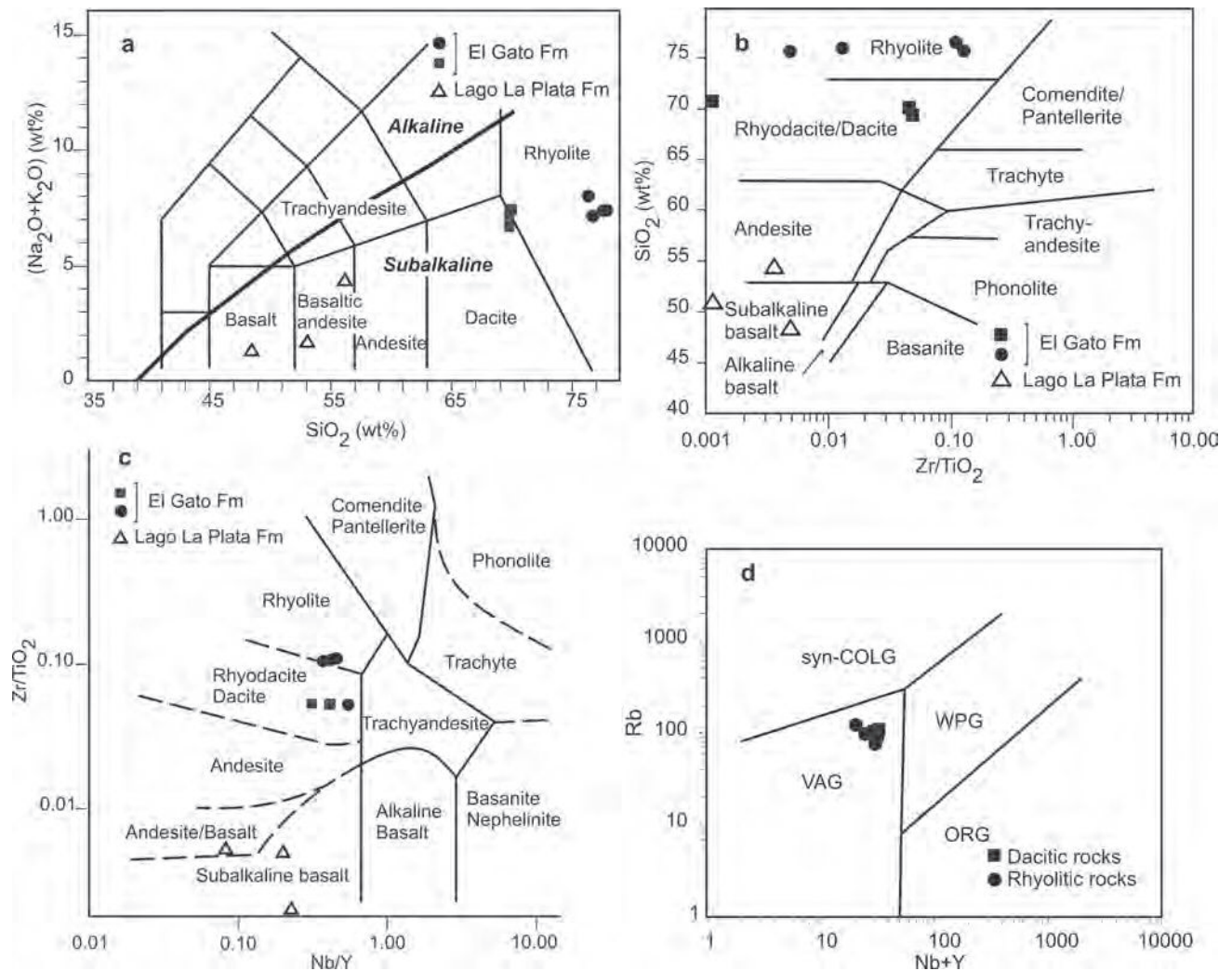
Fig. 3. Classification of igneous rocks in the study area: *a*. Total alkali vs. silica compositional classification diagram for volcanic rocks (Le Maitre et al., 2002); *b*. Volcanic rock classification diagram (after Winchester and Floyd, 1977); *c*. Zr/TiO$_2$ vs. Nb/Y volcanic rock compositional classification (after Winchester and Floyd, 1977); *d*. Rb vs. Nb+Y tectonic discrimination diagram (after Pearce et al., 1984) for El Gato igneous rocks.

brownish-gray hornfels containing an amphibole ± epidote ± chlorite ± quartz mineral assemblage. Soon after, exoskarn formation in the calcareous sandstone produced clinopyroxene ± garnet ± quartz ± epidote, followed by amphibole ± epidote ± chlorite ± quartz retrograde mineral assemblages. This paragenetic sequence is better recognized in open-cast working L3 (Figs. 2, 4), where a 5 m-thick exoskarn zone can be seen.

Compositional variations in clinopyroxene have been determined in the exoskarn facies between L3 and L4 (Fig. 2). Thus, in L3, a hedenbergitic pyroxene-rich zone, up to 1 m thick, was identified near the dacitic dike. It comprises <1 cm long, green prismatic hedenbergite crystals (Fig. 5a), and anisotropic zoned brown garnet (Fig. 5b), both partially retrograded to actinolite. In comparison, in open-cast working L4, electron microprobe analyses of clinopyroxene crystals from distal facies reveal a manganese enrichment, with up to 7.4 wt.% MnO and 20.4 wt.% FeO (Table 4, Fig. 6b). Manganese enrichment occurs as

coarse-grained brown Mn-hedenbergite, forming radiating-prismatic fibrous crystals up to 10 cm long, resulting in an irregular, 4 m-thick, metasomatic replacement body, locally preserving original calcareous sandstone remnants.

Other poorly developed exoskarn replacements have been recognized in Lago La Plata basaltic andesite along the contact with the intrusive rocks. The original pilotaxitic texture is overprinted by patches of coarse-grained amphibole, only a few millimeters wide, as well as scarce, very thin crosscutting fibrous actinolite veinlets.

Areas most exploited for iron occur in pits L5 and L6 (Fig. 2). Only a few exposures, up to 5 meters long and 4 m wide, still remain as irregular replacement masses of the sedimentary rocks. The magnetite is erratically distributed as small, high-grade pods and lenses. These bodies contain subhedral magnetite crystals with interstitial quartz, which include trace amounts of fine-grained pyrrhotite (5–15 µm) and pyrite (20 µm). The outer rims of these bodies are enriched in epidote > chlorite. Petrographic studies reveal a

Table 2. Representative Electron Microprobe Analyses of Pyroxenes: El Abuelo Endoskarn (L3)

	P32	P33	P34	P35	P36	P41	P42	P44	P45	P47	P50
Oxide Composition (wt. %)											
SiO_2	50.73	50.60	50.26	51.78	51.88	52.16	51.41	51.73	50.77	51.20	50.94
TiO_2	0.02	0.00	0.01	0.00	0.00	0.02	0.00	0.01	0.00	0.00	0.05
Al_2O_3	0.18	0.11	0.05	0.20	0.10	0.17	0.20	0.18	0.02	0.05	0.24
Cr_2O_3	0.00	0.00	0.00	0.00	0.01	0.04	0.00	0.00	0.02	0.00	0.00
Fe_2O_3	0.00	0.40	0.00	0.00	0.31	0.21	0.00	0.00	1.12	0.31	0.00
FeO	12.36	14.33	16.29	10.29	10.36	9.89	11.58	11.73	12.17	11.85	13.34
MnO	2.81	3.81	2.05	1.53	1.86	1.69	2.51	2.20	2.22	2.45	2.97
NiO	0.00	0.06	0.03	0.00	0.05	0.01	0.00	0.00	0.00	0.00	0.02
MgO	8.16	6.41	6.07	10.33	10.18	10.57	8.72	9.11	8.39	8.72	7.56
CaO	23.96	23.88	23.74	24.35	24.41	24.80	24.27	24.37	24.28	24.43	23.62
Na_2O	0.04	0.03	0.06	0.04	0.05	0.04	0.06	0.06	0.02	0.00	0.07
K_2O	0.00	0.02	0.01	0.01	0.00	0.00	0.00	0.00	0.01	0.00	0.00
Total	98.26	99.63	98.57	98.53	99.20	99.60	98.75	99.39	99.01	99.00	98.81
Number of Ions on the Basis of 6 Atoms of Oxygen											
Si	2.00	1.99	2.00	2.00	2.00	1.99	2.00	2.00	1.98	2.00	2.00
Al(IV)	0.00	0.01	0.00	0.00	0.00	0.01	0.00	0.00	0.00	0.00	0.00
Fe^{3+}	0.00	0.00	0.00	0.00	0.00	0.00	0.00	0.00	0.02	0.00	0.00
Sum	2.00	2.00	2.00	2.00	2.00	2.00	2.00	2.00	2.00	2.00	2.00
Al(VI)	0.01	0.00	0.00	0.01	0.00	0.00	0.01	0.01	0.00	0.00	0.01
Fe^{3+}	0.00	0.01	0.00	0.00	0.01	0.01	0.00	0.00	0.02	0.01	0.00
Ti	0.00	0.00	0.00	0.00	0.00	0.00	0.00	0.00	0.00	0.00	0.00
Cr	0.00	0.00	0.00	0.00	0.00	0.01	0.00	0.00	0.00	0.00	0.00
Fe^{2+}	0.41	0.47	0.55	0.34	0.33	0.32	0.39	0.39	0.40	0.39	0.46
Mn	0.09	0.13	0.07	0.05	0.06	0.05	0.08	0.07	0.07	0.08	0.10
Ni	0.00	0.00	0.00	0.00	0.00	0.00	0.00	0.00	0.00	0.00	0.00
Mg	0.48	0.38	0.36	0.60	0.58	0.60	0.51	0.53	0.49	0.51	0.44
Ca	1.01	1.01	1.01	1.01	1.01	1.02	1.01	1.01	1.02	1.02	1.00
Na	0.00	0.00	0.01	0.00	0.00	0.00	0.01	0.00	0.00	0.00	0.01
K	0.00	0.00	0.00	0.00	0.00	0.00	0.00	0.00	0.00	0.00	0.00
Sum	2.00	2.00	2.00	2.01	1.99	2.01	2.01	2.01	2.00	2.01	2.02
Total	4.00	4.00	4.00	4.01	3.99	4.01	4.01	4.01	4.00	4.01	4.02
Clinopyroxene Components (Mole Fraction)											
Hd	41.53	49.04	55.94	34.58	34.72	32.89	39.96	39.39	43.38	40.24	45.69
Dio	48.88	38.12	36.99	60.35	59.11	61.49	51.58	53.30	49.19	51.53	44.39
Jo	9.59	12.84	7.07	5.07	6.17	5.62	8.46	7.31	7.43	8.23	9.92
Total	100.00	100.00	100.00	100.00	100.00	100.00	100.00	100.00	100.00	100.00	100.00

Note

Measured using a Cameca Camebax SX50 electron microprobe, at the Departamento de Geología, Universidad de Oviedo, Spain. Operating conditions: accelerating voltage 20 kV, beam current at 20 mA.

Fe content (Fe^{2+} and Fe^{3+}) was recalculated following Droop (1987).

Abbreviations: Dio = diopside; Hd = hedenbergite; Jo = Johannsenite.

Table 3. Representative Electron Microprobe Analyses of Garnets: El Abuelo Endoskarn (L3)

	P13	P14	P17	P19	P22	P25	P27	P28	P29	P32	P33	P37	P41
Oxide Composition (wt. %)													
SiO_2	36.83	35.99	36.20	35.73	37.98	35.93	36.55	36.33	35.14	35.76	35.89	34.71	35.63
P_2O_5	0.04	0.05	0.04	0.04	0.03	0.02	0.03	0.03	0.03	0.02	0.03	0.02	0.09
TiO_2	0.09	0.02	0.00	0.09	0.23	0.01	0.07	0.00	0.00	0.44	0.08	0.01	0.01
Al_2O_3	2.84	3.62	5.54	2.71	10.25	2.20	5.85	5.06	1.54	10.84	4.69	1.46	1.58
Cr_2O_3	0.02	0.03	0.00	0.00	0.00	0.00	0.01	0.00	0.06	0.00	0.03	0.07	0.00
Fe_2O_3	25.75	24.95	22.91	25.28	15.63	26.02	21.21	22.66	27.51	15.19	24.09	28.75	26.92
FeO	0.00	0.44	0.17	1.11	1.38	1.24	1.14	0.72	0.16	0.00	0.00	0.05	1.08
MnO	0.19	0.31	0.27	0.68	1.25	0.19	0.28	0.18	0.24	1.98	0.30	0.12	0.23
MgO	0.14	0.14	0.10	0.17	0.08	0.09	0.13	0.08	0.20	0.03	0.14	0.01	0.21
NiO	0.05	0.05	0.00	0.00	0.04	0.00	0.03	0.00	0.06	0.00	0.00	0.05	0.00
CaO	32.93	34.07	34.28	33.03	33.71	33.59	33.69	34.13	34.00	33.32	34.39	34.04	33.48
Na_2O	0.01	0.01	0.02	0.01	0.01	0.01	0.00	0.00	0.00	0.00	0.00	0.00	0.00
K_2O	0.00	0.00	0.00	0.00	0.01	0.01	0.00	0.00	0.01	0.01	0.00	0.00	0.00
F	0.02	0.00	0.00	0.01	0.00	0.01	0.01	0.00	0.00	0.00	0.00	0.00	0.00
Cl	0.01	0.00	0.00	0.00	0.00	0.00	0.00	0.01	0.01	0.01	0.01	0.00	0.00
Total	98.92	99.68	99.53	98.86	100.60	99.32	99.00	99.20	98.96	97.60	99.65	99.29	99.23
Number of Ions on the Basis of 24 Atoms of Oxygen													
Si	6.18	5.97	5.95	6.00	6.04	6.02	6.02	5.99	5.92	5.85	5.91	5.86	6.00
P^{5+}	0.00	0.00	0.00	0.00	0.00	0.00	0.00	0.00	0.00	0.00	0.00	0.00	0.00
Al(IV)	0.00	0.03	0.05	0.00	0.00	0.00	0.00	0.01	0.08	0.15	0.09	0.14	0.00
Fe^{3+}	0.00	0.00	0.00	0.00	0.00	0.00	0.00	0.00	0.00	0.00	0.00	0.00	0.00
Sum	6.18	6.00	6.00	6.00	6.04	6.02	6.02	6.00	6.00	6.00	6.00	6.00	6.00
Al(VI)	0.60	0.73	1.10	0.58	2.00	0.47	1.21	1.04	0.25	1.03	0.89	0.17	0.34
Cr	0.00	0.00	0.00	0.00	0.00	0.00	0.00	0.00	0.01	0.00	0.00	0.01	0.00
Fe^{3+}	3.04	3.34	3.03	3.43	1.94	3.53	2.81	3.03	3.82	2.11	3.24	3.98	3.74
Ti	0.01	0.00	0.00	0.01	0.03	0.00	0.01	0.00	0.00	0.05	0.01	0.00	0.00
Sum	3.65	4.07	4.13	4.02	3.97	4.00	4.05	4.07	4.07	4.19	4.13	4.15	4.08
Mg	0.03	0.03	0.02	0.04	0.02	0.02	0.03	0.02	0.05	0.01	0.03	0.00	0.05
Fe^{2+}	0.00	0.07	0.02	0.17	0.19	0.19	0.17	0.11	0.02	0.00	0.00	0.01	0.16
Mn	0.03	0.04	0.04	0.10	0.17	0.03	0.04	0.03	0.03	0.27	0.04	0.02	0.03
Ni	0.00	0.01	0.00	0.00	0.00	0.00	0.00	0.00	0.00	0.00	0.00	0.01	0.00
Ca	5.92	6.05	6.06	5.96	5.75	6.04	5.95	6.06	6.19	5.87	6.11	6.16	6.05
Na	0.00	0.00	0.01	0.00	0.01	0.00	0.00	0.00	0.00	0.00	0.00	0.00	0.00
K	0.00	0.00	0.00	0.00	0.00	0.00	0.00	0.00	0.00	0.00	0.00	0.00	0.00
Sum	5.98	6.20	6.15	6.27	6.14	6.28	6.19	6.22	6.28	6.15	6.18	6.20	6.29
F	0.01	0.00	0.00	0.01	0.00	0.00	0.00	0.00	0.00	0.00	0.00	0.00	0.00
Cl	0.00	0.00	0.00	0.00	0.00	0.00	0.00	0.00	0.00	0.00	0.00	0.00	0.00
Total	15.82	16.27	16.28	16.29	16.15	16.30	16.26	16.29	16.35	16.34	16.31	16.35	16.37
Garnet Compounds (Mole Fraction)													
Pyp+Sp+Alm	1.03	2.33	1.43	4.90	6.19	3.77	3.86	2.47	1.74	4.58	1.23	0.45	3.97
Grs	15.44	15.55	25.20	9.51	44.57	7.97	26.15	23.16	4.45	44.52	20.32	3.75	4.25
Ad	83.53	82.12	73.37	85.59	49.24	88.26	69.99	74.37	93.81	50.90	78.45	95.80	91.78
Total	100.00	100.00	100.00	100.00	100.00	100.00	100.00	100.00	100.00	100.00	100.00	100.00	100.00

Note

Sample analysis as in Table 2.
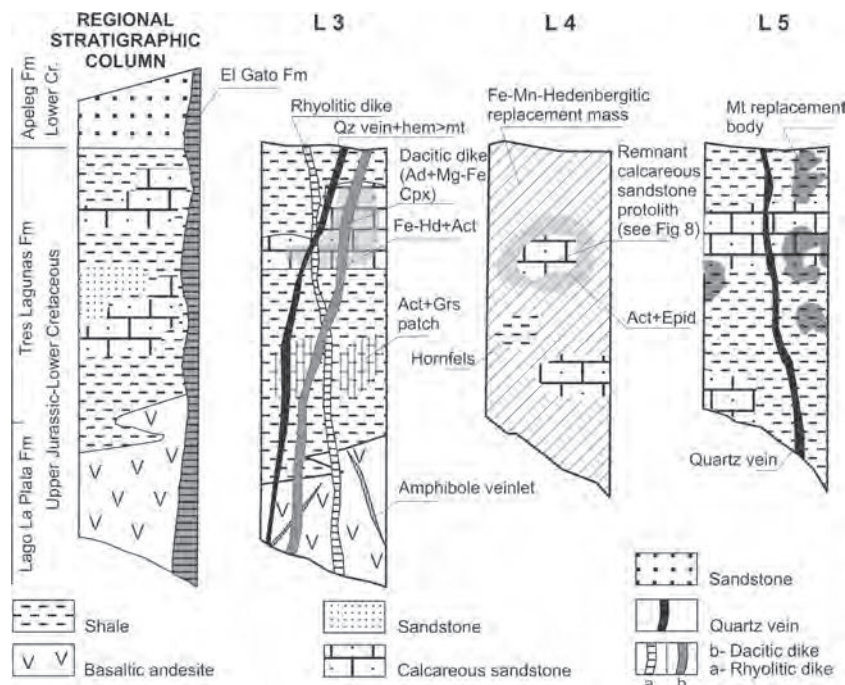Abbreviations: Ad = andradite; Alm = almandine; Grs = grossular; Pyp = pyrope; Sp = spessartine.

Fig. 4. Schematic stratigraphic columns with typical skarn alteration profiles of the El Abuelo mine through various parts (without scale). See Fig. 2 for locations of pits L3–L5. Abbreviations: Act = actinolite; Mg-Fe-Cpx = Mg-Fe-clinopyroxene; Epid = epidote; Grs = grossular; Fe-Hd = Fe-hedenbergite; Mt = magnetite.

finely banded texture of alternating quartz and magnetite layers. The magnetite crystal margins are usually replaced by hematite. Microprobe analyses of coarse-grained magnetite are shown in Table 5. They indicate that the magnetite comprises 30.1 to 30.5 wt.% FeO, 66.8 to 67.7 wt.% Fe_2O_3, and up to 0.16 wt.% MnO, with low TiO_2 contents ($\leq$0.02 wt.%).

Hydrothermal Processes
(Vein Stage)

Later, lower temperature hydrothermal alteration overprinted the earlier skarn assemblage. This was linked to the formation of late, near-vertical, coarse-grained, white quartz veins that are 0.5 to 1 m thick, and trend SE to ESE (Fig. 2). The veins are massive and are associated with several crosscutting quartz veinlets. Hydrothermal fluid activity at Cerro Pepita caused a propylitic outermost halo marked by (1) plagioclase replaced by epidote and calcite, (2) epidote, chlorite, and calcite replacing pyroxene and amphibole, and (3) patchy replacement of the volcanic groundmass and sedimentary matrix by calcite, epidote, chlorite, and clay minerals.

The veinlets contain an assemblage of quartz ± sericite ± adularia ± titanite ± hematite ± pyrite ± chalcopyrite > sphalerite ± galena. The adularia occurs as scarce intergrowths, forming rhombic crystals up to 50 μm, which is typical of epithermal environments (Dong and Morrison, 1995). Also, disseminated in the wall rock are small sericite-rich patches, as well as very scarce, 50 μm to 1 mm

long, xenomorphic grains of pyrite and chalcopyrite.

Towards the northern sector, in workings L8 and L9 (Fig. 2), the quartz veins also contain chalcedony and jasperoid, suggesting that late fluids were low temperature.

The El Solcito vein (Fig. 2) does not appear to be spatially associated with skarn. In this area, the Tres Lagunas sandstone and shale are cut by a 300 m, SE-trending brecciated quartz lode, 0.5 to 0.8 m thick, that contains Cu-Fe-sulfide-bearing veinlets.

Clay minerals (mostly kaolinite) were subsequently formed by supergene processes, as well as an incipient copper-iron gossan.

Assays of grab samples from the El Abuelo and El Solcito quartz veins show some anomalous quantities of Ag, Au, Cu, Pb, and Zn (Table 6). Maximum values include 81 ppm Ag and 0.05 ppm Au in sample 4260, and >1 wt.% base metals (Cu, Zn) in several samples.

Stable Isotopes

$\delta^{18}O_{H_2O}$ and δD_{H_2O} (Table 7) were calculated from isotopic measurements on two actinolite crystals from retrograde skarn facies at open cast working L3. $\delta^{18}O_{H_2O}$ measurements range between 2.07‰ and 2.27‰, whereas δD_{H_2O} ranges from −85‰ to −76‰ (recalculated using the fractionation equations of Zheng, 1993, and Graham et al., 1984, respectively, at 300ºC). Reference meteoric waters, employed to infer metallogenic conditions, were determined from the pluviometric database of the International Atomic Energy Agency (Vienna). These waters are considered to have similar paleolatitude, altitude, and continental conditions to those during the Cretaceous.

Sulfur isotopes ($\delta^{34}S_{CDT}$) of two samples of pyrite from El Abuelo (L5) and El Solcito quartz veinlets yielded values of +0.1‰ and +0.2‰, respectively (Table 7). $\delta^{34}S_{H_2S}$ was recalculated using the fractionation equation of Ohmoto and Rye (1979).

Comparison with Other Skarn and
IOCG Deposits

Many of the geological and alteration features present at the El Abuelo skarn resemble those in some other skarns in southwestern Mendoza province of Argentina (Franchini and Innes, 1997; Franchini and Dawson, 1999; Franchini et al., 2000, 2005). They are also comparable to features seen in the Zn-Pb-Cu-Au El Toqui ore deposit in Chile (Wellmer et al., 1983; Wellmer and Reeve, 1990; Kakarieka, 2003)

Table 4. Representative Electron Microprobe Analyses of Pyroxenes: El Abuelo Exoskarn (L4)

	P1	P2	P3	P4	P5	P7	P10	P11	P12
Oxide Composition (wt. %)									
SiO_2	48.40	47.54	47.43	47.21	48.97	48.15	47.56	47.34	47.89
Al_2O_3	0.48	0.44	0.44	0.46	0.57	0.15	0.17	0.15	0.54
Fe_2O_3	0.97	1.72	2.19	3.32	0.00	1.25	1.72	2.56	3.28
FeO	20.43	18.97	19.41	18.16	21.28	19.45	19.05	16.50	18.28
MnO	6.97	6.81	7.00	6.79	6.88	7.00	7.39	7.05	7.15
MgO	0.73	0.81	0.85	0.90	0.63	0.92	0.71	2.04	0.79
CaO	22.63	22.52	21.85	22.24	22.77	22.78	22.78	22.52	22.80
Na_2O	0.07	0.14	0.06	0.12	0.14	0.03	0.01	0.10	0.10
Total	100.68	98.95	99.23	99.20	101.24	99.73	99.39	98.26	100.83
Number of Ions on the Basis of 6 Atoms of Oxygen									
Si	1.90	1.89	1.89	1.88	1.90	1.98	1.97	1.96	1.88
Al(IV)	0.10	0.10	0.10	0.10	0.10	0.01	0.01	0.01	0.10
Fe^{3+}	0.00	0.01	0.01	0.02	0.00	0.01	0.02	0.03	0.02
Sum	2.00	2.00	2.00	2.00	2.00	2.00	2.00	2.00	2.00
Al(VI)	0.00	0.00	0.00	0.00	0.00	0.00	0.00	0.00	0.00
Fe^{3+}	0.03	0.05	0.06	0.09	0.00	0.03	0.03	0.05	0.09
Mg	0.04	0.05	0.05	0.06	0.04	0.06	0.04	0.13	0.05
Fe^{2+}	0.70	0.66	0.67	0.63	0.74	0.67	0.66	0.57	0.62
Mn	0.24	0.24	0.25	0.24	0.24	0.24	0.26	0.25	0.25
Ca	0.99	1.00	0.97	0.98	0.99	1.00	1.01	1.00	0.99
Na	0.01	0.01	0.00	0.01	0.01	0.00	0.00	0.01	0.01
Sum	2.01	2.01	2.00	2.01	2.02	2.00	2.00	2.01	2.01
Total	4.01	4.01	4.00	4.01	4.02	4.00	4.00	4.01	4.01
Clinopyroxene Components (Mole Fraction)									
Hd	71.87	71.10	71.28	71.37	72.87	70.23	70.21	63.59	71.12
Dio	4.34	4.98	5.07	5.42	3.76	5.54	4.31	12.30	4.68
Jo	23.79	23.92	23.65	23.21	23.37	24.23	25.48	24.12	24.20
Total	100.00	100.00	100.00	100.00	100.00	100.00	100.00	100.00	100.00

Notes
Sample analysis as in Table 2.
Pyroxene Fe content (Fe^{2+} and Fe^{3+}) was recalculated following Droop (1987).
Abbreviations: Dio = diopside; Hd = hedenbergite; Jo = Johannsenite.

and to some magnetite-rich skarn deposits in western British Columbia, Canada (Meinert, 1984).

Like the Mendoza skarns (e.g., Hierro Indio, Vegas Peladas, Poblet, El Kaiser), the El Abuelo deposit exhibits the following features: (1) a close association with calc-alkaline arc-related igneous rocks, (2) magnetite as the most abundant ore mineral, (3) Cu-Fe sulfides that are largely subordinate to magnetite, and (4) pyroxene-garnet-epidote as the principal calc-silicate mineral assemblage. Important differences of the Mendoza skarns include: (1) the deposits are emplaced in different stratigraphic units of the Mesozoic marine–continental sedimentary sequence, (2) the related igneous suite is andesitic to dioritic in composition, and (3) the suite is of Tertiary (Miocene) age. These

geological features are typical of the region north of 43ºS, in Mendoza and Neuquén provinces of Argentina, where Tertiary arc magmatism dominates metallogenetic events.

Eighty kilometers west of the El Abuelo deposit, in the Aysén province of the Chilean Andean Precordillera, the El Toqui district hosts the main Zn-Pb mineralization of southern Chile. These deposits are classified as skarns by Collao (1994) and Maksaev (2005), although a syngenetic volcanic origin was earlier proposed by Wellmer et al. (1983). The base metal sulfides are hosted by Lower Cretaceous tuffs and limestones of the Coyhaique Formation, which correlates with the Tres Lagunas Formation in Argentina. In this area, quartz-feldspar porphyry sills and dikes of Cretaceous age are closely associated with the stratiform

Table 5. Representative Electron Microprobe Analyses of Magnetites: El Abuelo Exoskarn (L5)

Oxide Composition (wt. %)														
	1/6	**1/20**	**2/9**	**2/13**	**2/14**	**2/16**	**3/8**	**3/9**	**3/10**	**3/13**	**3/15**	**3/16**	**3/18**	**3/19**
SiO_2	0.02	0.06	0.04	0.04	0.02	0.01	0.05	0.07	0.01	0.02	0.03	0.03	0.01	0.03
Al_2O_3	0.03	0.05	0.03	0.05	0.01	0.00	0.05	0.04	0.01	0.04	0.00	0.03	0.02	0.04
TiO_2	0.00	0.01	0.00	0.01	0.00	0.01	0.00	0.00	0.00	0.00	0.00	0.00	0.01	0.02
V_2O_3	0.02	0.02	0.01	0.00	0.02	0.00	0.01	0.00	0.01	0.03	0.00	0.00	0.00	0.00
Fe_2O_3	67.74	67.31	67.33	66.84	67.52	67.30	67.28	67.13	67.12	67.29	67.22	67.23	67.65	67.13
FeO	30.25	30.19	30.45	30.43	30.05	30.17	30.32	30.54	30.31	30.33	30.15	30.35	30.41	30.37
MgO	0.01	0.00	0.00	0.00	0.00	0.00	0.00	0.00	0.00	0.01	0.00	0.00	0.00	0.03
MnO	0.06	0.09	0.09	0.13	0.15	0.15	0.06	0.07	0.03	0.10	0.16	0.11	0.09	0.06
CaO	0.00	0.00	0.01	0.00	0.00	0.00	0.00	0.00	0.02	0.01	0.00	0.03	0.00	0.00
Cr_2O_3	0.01	0.00	0.00	0.00	0.00	0.00	0.01	0.02	0.00	0.01	0.01	0.04	0.02	0.01
Zn	0.00	0.01	0.10	0.12	0.02	0.00	0.03	0.07	0.10	0.15	0.00	0.06	0.00	0.04
Ni	0.00	0.00	0.01	0.06	0.02	0.00	0.05	0.05	0.00	0.01	0.06	0.03	0.04	0.00
Total	98.14	97.74	98.07	97.68	97.81	97.64	97.86	97.99	97.61	98.00	97.63	97.91	98.25	97.73
Number of Ions on the Basis of 4 Atoms of Oxygen														
	1/6	**1/20**	**2/9**	**2/13**	**2/14**	**2/16**	**3/8**	**3/9**	**3/10**	**3/13**	**3/15**	**3/16**	**3/18**	**3/19**
Si	0.00	0.00	0.00	0.00	0.00	0.00	0.00	0.00	0.00	0.00	0.00	0.00	0.00	0.00
Al	0.00	0.00	0.00	0.00	0.00	0.00	0.00	0.00	0.00	0.00	0.00	0.00	0.00	0.00
Ti	0.00	0.00	0.00	0.00	0.00	0.00	0.00	0.00	0.00	0.00	0.00	0.00	0.00	0.00
V	0.00	0.00	0.00	0.00	0.00	0.00	0.00	0.00	0.00	0.00	0.00	0.00	0.00	0.00
Fe^{3+}	2.00	1.99	1.99	1.99	2.00	2.00	1.99	1.99	1.99	1.99	2.00	1.99	2.00	1.99
Fe^{2+}	0.99	0.99	1.00	1.00	0.99	1.00	1.00	1.00	1.00	1.00	1.00	1.00	1.00	1.00
Mg	0.00	0.00	0.00	0.00	0.00	0.00	0.00	0.00	0.00	0.00	0.00	0.00	0.00	0.00
Mn	0.00	0.00	0.00	0.00	0.00	0.00	0.00	0.00	0.00	0.00	0.00	0.00	0.00	0.00
Ca	0.00	0.00	0.00	0.00	0.00	0.00	0.00	0.00	0.00	0.00	0.00	0.00	0.00	0.00
Cr	0.00	0.00	0.00	0.00	0.00	0.00	0.00	0.00	0.00	0.00	0.00	0.00	0.00	0.00
Zn	0.00	0.00	0.00	0.00	0.00	0.00	0.00	0.00	0.00	0.00	0.00	0.00	0.00	0.00
Ni	0.00	0.00	0.00	0.00	0.00	0.00	0.00	0.00	0.00	0.00	0.00	0.00	0.00	0.00
Total	2.99	2.98	2.99	2.99	2.99	3.00	2.99	2.99	2.99	2.99	3.00	2.99	3.00	2.99

Note

Determined with a Cameca Camebax SX50 electron microprobe at the Departamento de Geología, Universidad de Oviedo, Spain. Operating conditions: accelerating voltage = 15 kV, beam current = 15 mA.

Element site allocation, and Fe^{2+}–Fe^{3+} recalculation based on computer program of the Departamento de Geología, Universidad de Río Cuarto, Argentina.

Table 6. Precious and Base Metal Contents of Quartz Veins

Sample	4259	4260	4267	4269	4274	4275
Au *(ppm)*	0.02	0.05	0.01	0.02	0.02	0.02
Ag	51.00	81.09	66.2	5.04	23.05	0.09
As	220	163	70	133	279	338
Cu	>10 000	>10 000	5070	>10 000	9307	399
Hg	<2	<2	<2	<2	4	4
Mo	5	6	20	12	12	3
Ni	9	12	7	16	11	16
Pb	1192	3521	5666	133	254	59
Sb	<5	<5	<5	<5	<5	<5
Sn	27	40	286	43	81	56
W	<20	27	<20	<20	<20	<20
Zn	3654	8708	>10 000	212	3168	801

Notes

Sample locations shown in Fig. 2.

Data obtained by fire assay-AA (Au; detection limit 0.01 ppm) and ICP-AES (inductively coupled plasma-atomic emission spectrometry) for the other elements. Alex Stewart Assayers Argentina S.A.

Table 7. O, H, and S Isotopic Determinations at the Pepita Hill Deposits

Sample	Location	Mineral	$\delta^{18}O_{min}$ (‰)	$\delta^{18}O_{H_2O}$ (‰)	δD_{min} (‰)	δD_{H_2O} (‰)
4249-1*	surface working L3	Actinolite	2.10	2.07	–113.8	–85.0
4249-2*	surface working L3	Actinolite	2.30	2.27	–105.0	–76.0
			$\delta^{34}S_{min}$ (‰)		$\delta^{34}S_{H_2S}$ (‰)	
4231	surface working L5	Pyrite	0.1		–1.2	
4247	El Solcito vein	Pyrite	0.2		–1.2	

Notes

*Data from Lanfranchini (2004).

ore deposits (Wellmer and Reeve, 1990). Although there are some spatial and temporal similarities between the El Toqui and El Abuelo deposits, such as similar stratigraphy and some mineralization styles, El Toqui shows several differences, such as higher contents of base metal sulfides, and a much thicker volcano-sedimentary protolith.

Unlike the calcic iron skarn deposits of western Canada described by Meinert (1984), which are hosted in oceanic island-arc terranes (Einaudi et al., 1981; Meinert, 1992), all the Argentinean Fe skarns were emplaced in a continental magmatic arc environment.

Some IOCG deposits described by Barton and Johnson (2000), Hitzman (2000), Pollard (2000), and Corriveau (2005), and especially several South American Andean IOCG deposits (e.g., Panulcillo, San Antonio, and La Farola, Chile) reported by Ray and Lefebure (2000), Sillitoe (2003), and Williams et al. (2005) display the following features, which are also observed in the El Abuelo skarn: (1) a receptive Jurassic–Cretaceous sedimentary sequence with interbedded basaltic andesite volcanic rocks, cut by high-angle faults creating structural permeability; (2) some exposures of contact metamorphism (hornfels) and calc-silicate alteration, with metasomatic aureoles developed around rhyolitic–dacitic dikes; (3) pervasive hydrothermal alteration; (4) irregular and incipient development of disseminated pyrite; (5) the existence of massive magnetite bodies hosted by exoskarn; (6) low TiO_2 (≤0.02 wt.%) content in the magnetite; and (7) trace amounts of base metal sulfides.

Petrogenetic Considerations

Although widespread Early Cretaceous sedimentary marine–continental sequences occur in southwest Chubut province, the Tres Lagunas calcareous sandstone protolith is confined to what were once shallow basins. Thus, exoskarn mineralogies were only observed at Cerro Pepita, where several favorable geological conditions existed.

Any genetic model for the El Abuelo deposit must account for the following geologic and metallogenic aspects: (1) close spatial relationship between the skarn deposit and the rhyolitic-dacitic dikes; (2) host-rock composition and stratigraphic control of the skarn; (3) the genetic connection between fracture-related permeability and mineralization; and (4) a late hydrothermal activity.

An intrusion-related model of the El Abuelo deposit is schematically shown in Figure 7, where skarn development follows the emplacement of the Cretaceous dikes in the Tres Lagunas sedimentary rocks. Skarn extends mainly in chemically reactive calcareous siliciclastic horizons, in direct contact with the two different types of dikes. The intrusions caused an initial isochemical, high-temperature contact metamorphism, represented by recrystallized hornfelsic rocks. During an early stage in the skarn formation, ascending magmatic-derived fluids caused metasomatic replacements in the calcareous sandstone and in the dacitic dike. Subsequently, the magmatic fluids, after mixing with meteoric waters, caused some retrograde replacement of the skarn. According to Bowman (1998), a moderate
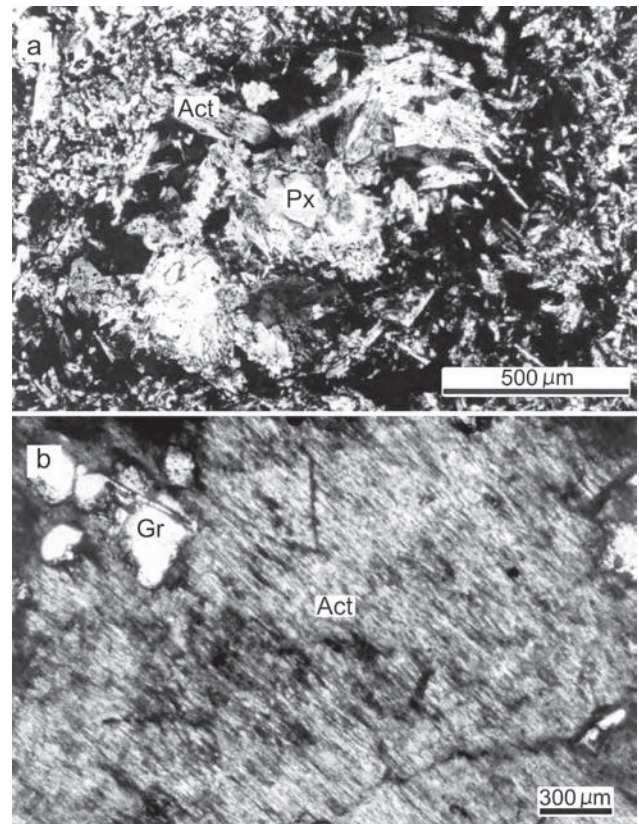

Fig. 5. Photomicrographs of: *a*. pyroxene partially altered to actinolite, from pit L3; *b*. garnet crystals included in actinolite, sample 4262; retrograde skarn stage. Transmitted cross-polarized light. Abbreviations: Act = actinolite; Gr = garnet; Px = pyroxene.

amount of mixing of magmatic fluids with meteoric waters is consistent with the $\delta^{18}O_{H_2O}$ and δD_{H_2O} determinations reported above.

Magnetite mineralization is spatially related to the hydrous mineral assemblages formed during the late retrograde stage of skarn formation. The Lago La Plata Fe-rich basaltic andesite wall rock could have been a source for the iron in the El Abuelo skarn. Finally, the whole sequence including the skarnified rocks was cut by epithermal quartz sulfide veins along ESE-trending fractures.

The close spatial relationship between the rhyolitic–dacitic dikes, skarn, and quartz veins, as well as sulfur isotopic compositions, are compatible with a magmatic sulfur source (Bowman, 1998), suggesting a magmatic-hydrothermal origin for the mineralizing fluids.

Conclusions

1. El Abuelo calcic iron skarn formed in a Mesozoic Andean continental magmatic arc tectonic setting.
2. The skarn originated from contact metasomatic processes related to magmatic hydrothermal activity associated with the intrusion of Early Cretaceous rhyolitic and dacitic dikes. The dikes are probably related to a larger
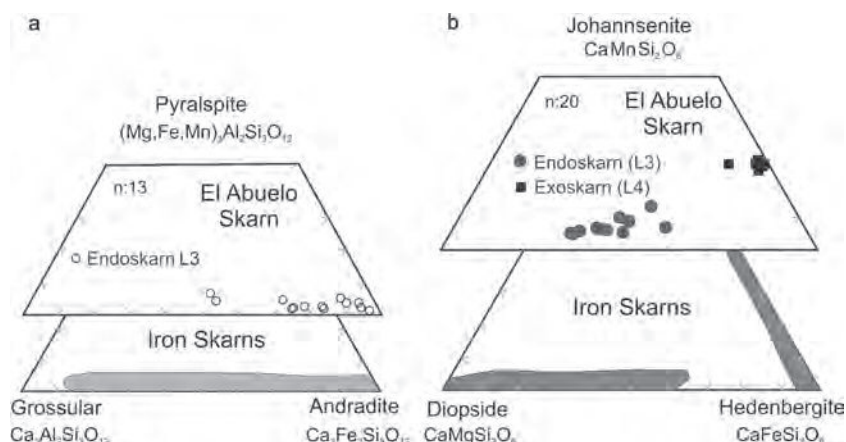
Fig. 6. Ternary diagrams of **a.** the El Abuelo skarn Ca Al-Ca Fe-(Mg Mn) Al garnet and **b.** Mg-Fe-Mn calcic pyroxene chemical compositions. Compositional fields (in gray) for garnet and pyroxene of Fe skarns are from Meinert (1984).

intrusive system at depth.

3. The distribution of the calc-silicate skarn and magnetite bodies was controlled by the lithological composition and structurally related permeability of the Tres Lagunas carbonate-siliciclastic sequence.

4. An initial recrystallization phase included hornfels generation followed by the two main stages of skarn formation: an early anhydrous prograde stage with Ca-garnet and Ca-Fe- and Fe-Mn-clinopyroxenes (exoskarn), and Fe-garnet and Mg-Fe-clinopyroxene (endoskarn) mineral assemblages; and a retrograde stage that resulted in actinolite-quartz-epidote-chlorite > sericite, and magnetite-hematite > pyrite-chalcopyrite mineral assemblages.

5. Post-skarn epithermal quartz veins contain anomalous Au, Ag, and Cu contents.

6. Major and trace element geochemical data for the rhyolitic and dacitic dikes show that the parental magma was of a moderately peraluminous, calc-alkaline volcanic arc affinity.

7. The El Abuelo deposit is the only mineralized skarn currently known in SW Chubut province, although other igneous bodies are present throughout the region.

8. The current evidence suggests the El Abuelo deposit is a contact metasomatic calcic Fe-skarn related to Cretaceous intrusive activity, although some metallogenic characteristics at Pepita Hill are similar to
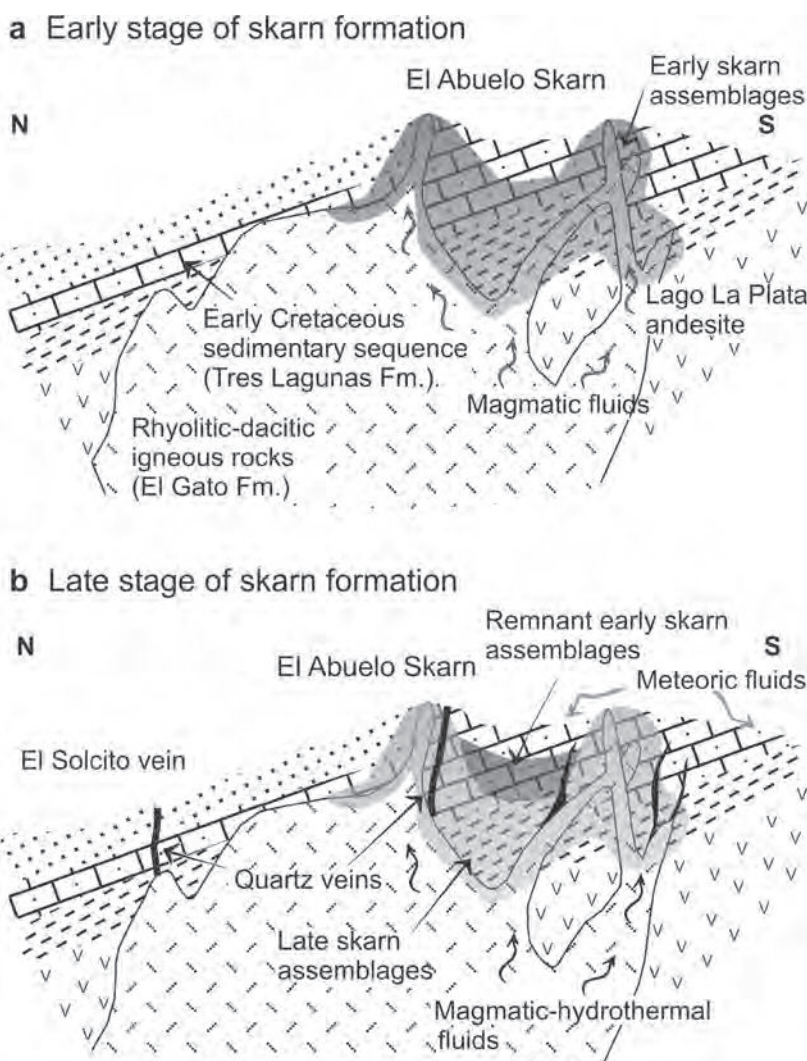

Fig. 7. Idealized cross sections of **a.** early, and **b.** late petrogenetic evolution of magmatic hydrothermal system at El Abuelo skarn (not to scale). Legend as in Fig. 4.

the Laboratorio de Isótopos Estables, Facultad de Ciencias, Universidad de Salamanca, Spain. Finally, we thank D.R. Lentz for his continuing encouragement and constructive comments on this paper.

References

Angelelli, V., 1984, Yacimientos metalíferos de la República Argentina: Comisión de Investigaciones Científicas de la Provincia de Buenos Aires (CICBA), v. 1, 191 p.

Barton, M.D., and Johnson, D.A., 2000, Alternative brine sources for Fe-oxide (Cu-Au) systems: Implications for hydrothermal alterations and metals, *in* Porter, T.M., ed., Hydrothermal iron oxide copper-gold & related deposits: A global perspective: Adelaide, Porter Geological Publishing, v. 1, p. 43–60.

Bowman, J., 1998, Stable-isotope systematics of skarns, *in* Lentz, D., ed., Mineralized intrusion related skarn systems: Mineralogical Association of Canada, Short Course Series, p. 99–144.

Canafoglia, M., Ramis, A., Botto, L., Cabello, C., Lanfranchini, M., Schalamuk, I., and Minelli, G., 2002, Efecto térmico y del ambiente reductor sobre la estabilidad de un mineral de la serie hedenbergita-johansenita: 6º Reunión de Mineralogía y Metalogénesis, La Plata, October 4–6, 2002, p. 57–62.

Clayton, R., and Mayeda, T., 1963, The use of bromine pentafluoride in the extraction of oxygen from oxides and silicates for isotopic analysis: Geochimica et Cosmochimica Acta, v. 27, p. 43–52.

Collao, S., 1994, Inclusiones fluidas en la formación de los yacimientos de Zn-Pb-Cu-Ag de El Toqui, XI Región Chile: 7º Congreso Geológico Chileno, Concepción, Chile, October, 1994, v. 2, p. 766–770.

Corriveau, L., 2005, Mineral deposits of Canada: Iron oxide copper-gold (± Ag ± Nb ± REE ± U) deposits: A Canadian perspective: URL <http://gsc.nrcan.gc.ca/mindep/synthdep/iocg/indexe.php>, 41 p. {June 2006}.

Dawson, K., Franchini, M., Cravero, O., Zanettini, J.C., and Márquez, M., 2000, Skarn deposits in Argentina; Studies in La Rioja, San Juan, Mendoza, Neuquén, and Chubut provinces: Servicio Geológico Minero Argentino, Biblioteca del Servicio Geológico Minero, Buenos Aires, Recursos Minerales 12, 165 p.

Dong, G., and Morrison, G., 1995, Adularia in epithermal veins, Queensland: Morphology, structural state, and origin: Mineralium Deposita, v. 30, p. 11–49.

Droop, G., 1987, A general equation for estimating Fe^{3+} concentrations in ferromagnesian silicates and oxides from microprobe analyses, using stoichiometric criteria: Mineralogical Magazine, v. 51, p. 431–435.

Einaudi, M., Meinert, L., and Newberry, R., 1981, Skarn deposits: Economic Geology 75th Anniversary Volume, p. 317–391.

Folguera, A., Vieira, J., and Gómez, A., 2000, Evolución Geológica de los Andes del Lago La Plata (45ºS): 9º Congreso Geológico Chileno, Puerto Varas, July 31–August 4, 2000, v. 2, p. 197–200.

Franchini, M.B., 2005, World skarn deposits: Skarns of Argentina, Economic Geology 100th Anniversary Volume, p. 299–336.

Franchini, M., and Dawson, K., 1999, Manifestaciones metálicas asociadas a skarns del sudoeste de Mendoza y noroeste del Neuquén: Recursos minerales de la República Argentina, Anales 35, p. 1535–1545.

Franchini, M., and Innes, A., 1997, Potencial aurífero de los skarns en contacto con las rocas ígneas de Quebrada Mala y áreas adyacentes, Neuquén, Argentina: 8° Congreso Geológico Chileno, Antofagasta, October 13–17, 1997, v. 2, p. 972–977.

Franchini, M., Meinert, L., and Montenegro, T., 2000, Skarn related porphyry-style mineralization at Caicayén Hill, Neuquén, Argentina: Composition and evolution of hydrothermal fluids: Economic Geology, v. 95, p. 1197–1213.

Franchini, M., de Barrio, R.E., Ríos, F.J., Schalamuk, I.B., Lanfranchini, M.E., and Pons, M.J., 2005, Petrología, Química mineral y paragénesis del depósito Hierro Indio, Mendoza: Guías para la exploración de skarns de Fe: 16º Congreso Geológico Argentino, La Plata, September 20–23, 2005, v. 2, p. 303–318.

Graham, C., Harmon, R., and Sheppard, S., 1984, Experimental hydrogen isotope studies: Hydrogen isotope exchange between amphibole and water: American Mineralogist, v. 69, p. 128–138.

Hayase, K., and Labudía, C., 1972, Presencia de manganohedenbergita en el Yacimiento de Hierro, Mina El Abuelo, Departamento Río Senguerr, Provincia del Chubut, República Argentina: Asociación Argentina de Mineralogía, Petrología y Sedimentología, v. 3, p. 27–34.

Hayase, K., Gelós, E., and Labudía, C., 1972, El Yacimiento de hierro Mina El Abuelo, Alto Río Senguerr, Provincia del Chubut, República Argentina: 5º Congreso Geológico Argentino, Córdoba, October 22–28, 1972, v. 2, p. 123–136.

Hitzman, M.W., 2000, Iron oxide Cu-Au deposits: What, where, when, and why, *in* Porter, T.M., ed., Hydrothermal iron oxide copper-gold and related deposits: A global perspective: Adelaide, Porter Geological Publishing, v. 1, p. 9–25.

Kakarieka, A., 2003, Exploración y descubrimiento del depósito de zinc Estatuas, Distrito Toqui, Aysen, Chile: 10° Congreso Geológico Chileno, Concepción, Chile, October 6–10, 2003, in CD-ROM, 10 p.

Lanfranchini, M.E., 2002, Rasgos geológicos y metalogénesis de la Sierra de Payaniyeu y sus alrededores, Provincia del Chubut, Argentina: Unpublished Tesis Doctoral, Facultad de Ciencias Naturales y Museo, Universidad Nacional de La Plata, 222 p.

Lanfranchini, M.E., 2004, Caracterización geológica del skarn "El Abuelo", Alto Río Senguerr, Chubut: Asociación Geológica Argentina, v. 59, p. 685–692.

Le Maitre, R., Streckeisen, A., Zanettin, B., Le Bas, M.J., Bonin, B., Bateman, P., Bellieni, G., Dudek, A., Efremova, S., Keller, J., Lameyre, J., Sabine, P.A., Schmid, R., Sorensen, H., and Woolley, A.R., 2002, Igneous rocks: A classification and glossary of terms; Recommendations of the International Union of Geological

Sciences, *in* Le Maitre, R., ed., Subcommission on the systematics of igneous rocks, 2nd ed.: Cambridge University Press, 236 p.

Maksaev, V., 2005, World skarn deposits: Skarns of Chile: Economic Geology 100th Anniversary Volume, p. 299–336.

Medina, A., and Maisterrena, E., 1981, De las mineralizaciones de las minas El Solcito y El Abuelo y su relación con la eruptividad, Departamento Río Senguerr, Provincia del Chubut: 8º Congreso Geológico Argentino, San Luis, September 20–26, 1981, v. 4, p. 571–581.

Meinert, L., 1984, Mineralogy and petrology of iron skarns in western British Columbia, Canada: Economic Geology, v. 79, p. 869–882.

Meinert, L., 1992, Skarns and skarn deposits: Geoscience Canada, v. 19, p. 145–162.

Méndez, V., Zanettini, J., and Zappettini, E., 1995, Geología y metalogénesis del orógeno Andino central, República Argentina: Dirección Nacional del Servicio Geológico, Secretaría de Minería de la Nación, Buenos Aires, Anales 23, 190 p.

Ohmoto, H., and Rye, R.O, 1979, Isotope of sulfur and carbon, *in* Barnes, H.L., ed., Geochemistry of hydrothermal ore deposits: New York, Wiley, p. 509–567.

Pearce, J.A., Harris, N., and Tindle, A., 1984, Trace elements discrimination diagram for the tectonic interpretation of granitic rocks: Journal of Petrology, v. 25, p. 956–983.

Ploszkiewicz, J., 1987, Descripción geológica de la Hoja 47 c, Apeleg, Provincia del Chubut: Dirección Nacional de Minería y Geología, Buenos Aires, Boletín N° 204, 100 p.

Ploszkiewicz, J., and Ramos, V.A., 1977, Estratigrafía y tectónica de la Sierra de Payaniyeu (Provincia del Chubut): Revista de la Asociación Geológica Argentina, v. 32, p. 209–226.

Pollard, P.J., 2000, Evidence of a magmatic fluid and metal source for Fe-oxide Cu-Au mineralization, *in* Porter, T.M., ed., Hydrothermal iron oxide copper-gold and related deposits: A global perspective: Adelaide, Porter Geological Publishing, v. 1, p. 27–41.

Ramos, V., 1976, Estratigrafía de los Lagos Fontana y La Plata (Chubut), Argentina: 1º Congreso Geológico Chileno, Santiago de Chile, August 2–7, 1976, v. 1 (A), p. 43–64.

Ramos, V., 1981, Descripción geológica de la Hoja 47 a b "Lago Fontana". Provincia del Chubut: Servicio Geológico Nacional, Buenos Aires, Boletín N° 183, 156 p.

Ramos, V., 1993, Interpretación tectónica, *in* Ramos V.A., ed., Geología y Recursos Naturales de Mendoza: 12º Congreso Geológico Argentino, Mendoza, October 10–15, 1993, v. 2, Congreso de Exploración de Hidrocarburos, Relatorio, I-19, p. 257–266.

Ray, G.E., and Lefebure, D.V., 2000, A synopsis of iron oxide $\pm$ Cu $\pm$ Au $\pm$ P $\pm$ REE deposits of the Candelaria-Kiruna-Olympic Dam family: British Columbia Ministry of Energy and Mines, Paper 2000-1, p. 267–272.

Robinson, B.W., and Kusakabe, M., 1975, Quantitative preparation of sulfur dioxide for $^{34}S/^{32}S$ analyses from sulfides by combustion with cuprous oxide: Analytical Chemistry, v. 47, p. 1179–1181.

Sillitoe, R.H., 1974, Tectonic segmentation of the Andes: Implications for magmatism and metallogeny: Nature, v. 250, p. 542–545.

Sillitoe, R.H., 2003, Iron oxide copper-gold deposits: An Andean view: Mineralium Deposita, v. 38, p. 787–812.

Wellmer, F.W., Reeve, E.J., Wentzlau, E., and Westenberger, H., 1983, Geology and ore deposits of the Toqui district, Aysen, Chile: Economic Geology, v. 78, p. 1119–1143.

Wellmer, F.W., and Reeve, E.J, 1990, The Toqui zinc-lead-copper-silver deposits, Aysén province, Chile, *in* Fontboté, L., Amstutz, G.C., Cardozo, M., Cedillo, E., and Frutos, J., eds., Stratabound ore deposits in the Andes: Berlin, Heidelberg, Springer-Verlag, p. 473–484.

Williams, P.J, Barton, M.D., Johnson, D.A., Fontboté, L., de Haller, A., Mark, G., Oliver, N.H.S., and Marschik, R., 2005, Iron oxide copper-gold deposits: Geology, space-time distribution, and possible modes of origin: Economic Geology 100th Anniversary Volume, p. 371–405.

Winchester, J.A., and Floyd, P.A., 1977, Geochemical discrimination of different magma series and their differentiation products using immobile elements: Chemical Geology, v. 20, p. 325–343.

Zheng, Y., 1993, Calculation of oxygen isotope fractionation in hydroxyl-bearing silicates: Earth and Planetary Science Letters, v. 120, p. 247–263.